Analytical and numerical solutions for a single vertical drain including the effects of vacuum preloading

Buddhima Indraratna, Cholachat Rujikiatkamjorn, and Iyathurai Sathananthan

Abstract: A system of vertical drains combined with vacuum preloading is an effective method to accelerate soil consolidation by promoting radial flow. This study presents the analytical modeling of vertical drains incorporating vacuum preloading in both axisymmetric and plane strain conditions. The effectiveness of the applied vacuum pressure along the drain length is considered. The exact solutions applied on the basis of the unit cell theory are supported by finite element analysis using ABAQUS software. Subsequently, the details of an appropriate matching procedure by transforming permeability and vacuum pressure between axisymmetric and equivalent plane strain conditions are described through analytical and numerical schemes. The effects of the magnitude and distribution of vacuum pressure on soft clay consolidation are examined through average excess pore pressure, consolidation settlement, and time analyses. Lastly, the practical implications of this study are discussed.

Key words: consolidation, finite element method, soft clay, vacuum preloading, vertical drains.

Résumé : Un système de drains verticaux combiné à du préchargement par vide est une méthode efficace d'accélérer la consolidation du sol en favorisant l'écoulement radial. Cette étude présente la modélisation analytique de drains verticaux incorporant le préchargement par vide pour des conditions d'axisymétrie et de déformation plane. On considère l'efficacité de la pression de vide appliquée tout le long du drain. Les solutions exactes utilisées sur la base de la théorie de la cellule unitaire sont appuyées par l'analyse en éléments finis au moyen du logiciel ABAQUS. Subséquemment, on décrit au moyen de procédés analytiques et numériques les détails d'une procédure appropriée d'appariement en transformant la perméabilité et la pression de vide entre les conditions d'axisymétrie et de déformation plane équivalente. On examine les effets de la grandeur et de la distribution de la pression de vide sur la consolidation de l'argile au moyen de l'excédent moyen de pression interstitielle, des analyses du tassement dû à la consolidation et du temps. Finalement, on discute les implications pratiques de cette étude.

Mots clés : consolidation, méthode d'éléments finis, argile molle, préchargement par vide, drains verticaux.

[Traduit par la Rédaction]

Introduction

In recent years, the construction of highway and railway embankments over unconsolidated soft soil deposits has resulted in the advancement of soil improvement techniques. To avoid excessive total and differential settlement of highly compressible soil, the application of preloading is regarded as one of the classical and popular methods in practice. Preloading is the application of surcharge load on the site prior to the placement of the permanent structure until most of the primary consolidation is achieved. In the case of thick soil deposits with low permeability, however, the consolidation time by preloading alone is considerably long, and hence a system of vertical drains is often introduced to achieve accelerated radial drainage and consolidation (Nicholson and Jardine 1982). The performance of various types of vertical drains including sand drains, sand compaction piles, prefabricated vertical drains (geosynthetic), and gravel piles has been studied in the past (Richart 1957; Cooper and Rose 1999; Indraratna et al. 1999). The use of prefabricated vertical drains with vacuum application is cost-effective, and the height of the surcharge embankment can be reduced to achieve the same consolidation settlement (Holtz et al. 1991; Shang et al. 1998). The mechanism of vacuum-assisted consolidation is comparable to, but not the same as, conventional surcharge. In earlier studies, vacuum preloading was often simulated with an equivalent surface load or by modifying the surface boundary condition. Laboratory observations confirm, however, that the vacuum pressure propagates downwards along the drains (trapezoidal distribution) in addition to the uniformly applied surface suction. Indraratna et al. (2004) explained this modeling approach in a recent paper. The rate of consolidation attributed to vacuum-assisted preloading is greater than that attributed to the conventional method because of the increase in the lateral hydraulic gradient.

To analyze the behaviour of vertical drains, the unit cell theory representing a single drain surrounded by a soil annu-

Received 15 July 2004. Accepted 27 January 2005. Published on the NRC Research Press Web site at http://cgj.nrc.ca on 16 August 2005.

B. Indraratna,[1] C. Rujikiatkamjorn, and I. Sathananthan. Faculty of Engineering, University of Wollongong, Wollongong, NSW 2522, Australia.

[1]Corresponding author (e-mail: indra@uow.edu.au).

Fig. 1. Conversion of axisymmetry radial flow adopted for analytical solutions: (*a*) vertical drain installation layout, (*b*) vertical drain in plane strain model, (*c*) axisymmetric unit cell, (*d*) plane strain unit cell.

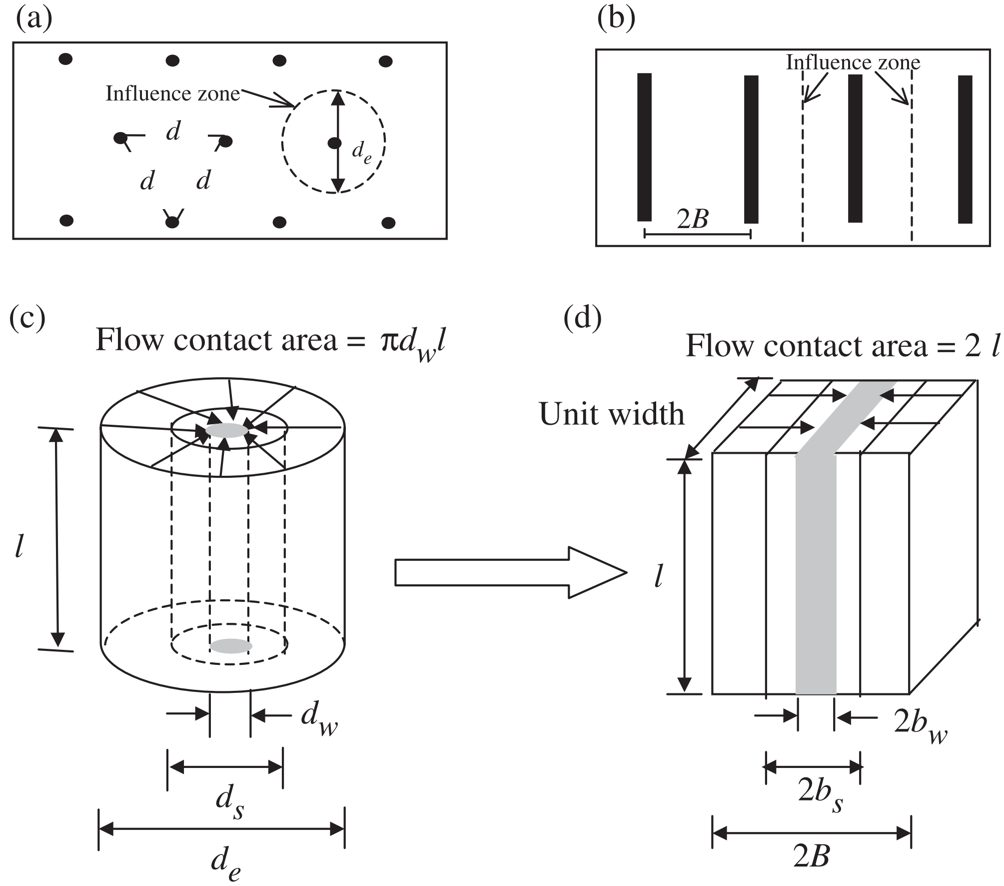

lus in axisymmetric condition (three-dimensional, 3D) was proposed by Barron (1948) and Richart (1957). Subsequently, Hird et al. (1992) introduced a unit cell formulated for the plane strain condition (two-dimensional, 2D), which can be more conveniently simulated in numerical modeling. For multidrain simulation, the plane strain finite element analysis can be readily adapted to most field situations (Hansbo 1981, 1997; Indraratna and Redana 1997, 2000). Nevertheless, realistic field predictions require the axisymmetric properties to be converted to an *equivalent* 2D plane strain condition, especially with regard to the permeability coefficients and drain geometry (Indraratna and Redana 1997). The plane strain analysis can also accommodate vacuum preloading in conjunction with vertical drains (e.g., Gabr and Szabo 1997). Mohamedelhassan and Shang (2002) discussed the application of vacuum pressure and its benefits, but without any vertical drains. The simulation of vacuum pressure for the vertical drain system in analytical or numerical models requires further refinement to obtain better predictions in the field.

The main objective of this paper is to introduce comprehensive analytical solutions for vacuum preloading in conjunction with vertical drains, in both the axisymmetric and equivalent plane strain conditions. The finite element model (FEM) ABAQUS (ABAQUS, Inc. 2004) incorporating these solutions is then validated for the single-drain situation. This finite element simulation also gives confidence to the users that an FEM code such as ABAQUS capturing the authors' theoretical formulations can then be extended to analyze multidrain case studies, given the convincing validation for a single-drain condition. It is to be noted, however, that demonstrating the ABAQUS application for multidrain field situations is not within the scope of this paper.

Analytical solution for a vertical drain without vacuum preloading

The analytical solutions are based on the equal-strain concept and are divided into two categories, namely axisymmetric and plane strain. For a single-drain analysis, the effects of well resistance and smear zone are included. Figure 1 illustrates the unit cell adopted for analytical solutions for the axisymmetric and plane strain conditions.

The main assumptions in this analysis are summarized as follows:

(1) The soil is fully saturated and homogeneous, and laminar flow through the soil (Darcy's law) is adopted. Flow is not permitted at the outer boundary of the unit cell, and only radial (horizontal) flow is permitted for relatively long vertical drains.

(2) For relatively small increments of effective stress ($d\sigma'$), radial consolidation theory (Barron 1948) is followed and a vertical drain is installed in saturated clay.

(3) Based on the equal-strain concept (Barron 1948), all vertical strains at any given depth z are assumed to be equal, and compressive strains are allowed to occur in the vertical direction only. The permeability of the soil is assumed to be constant during consolidation.

Axisymmetric condition

The governing equation for radial consolidation (Barron 1948) can be expressed by

$$[1] \qquad c_{\mathrm{h}}\left(\frac{1}{r}\frac{\partial u}{\partial r}+\frac{\partial^2 u}{\partial r^2}\right)=\frac{\partial u}{\partial t}$$

where c_{h} is the coefficient of consolidation for horizontal drainage, u is the excess pore-water pressure, r is the distance from the centre of the drain in the axisymmetric unit cell, and t is the time.

The solution for eq. [1] is given by (modified after Hansbo 1981)

$$[2a] \qquad \frac{\bar{u}}{\sigma_1}=\exp\left(\frac{-8T_{\mathrm{h,ax}}}{\mu_{\mathrm{ax}}}\right)$$

where

$$[2b] \qquad \mu_{\mathrm{ax}}=\frac{n^2}{n^2-1}\left[\ln\left(\frac{n}{s}\right)+\frac{k_{\mathrm{h,ax}}}{k_{\mathrm{s,ax}}}\ln(s)-\frac{3}{4}\right]+\frac{s^2}{n^2-1}\times\left(1-\frac{s^2}{4n^2}\right)+\frac{k_{\mathrm{h,ax}}}{k_{\mathrm{s,ax}}}\frac{1}{n^2-1}\left(\frac{s^4-1}{4n^2}-s^2+1\right)+\pi\frac{2k_{\mathrm{h,ax}}}{3q_{\mathrm{w}}}l^2\left(1-\frac{1}{n^2}\right)\approx\left[\ln\left(\frac{n}{s}\right)+\frac{k_{\mathrm{h,ax}}}{k_{\mathrm{s,ax}}}\ln(s)-\frac{3}{4}+\pi\frac{2k_{\mathrm{h,ax}}}{3q_{\mathrm{w}}}l^2\right]$$

and

$$[2c] \qquad T_{\mathrm{h,ax}}=c_{\mathrm{h,ax}}t/d_{\mathrm{e}}^2$$

where $\bar{u}$ is the average excess pore-water pressure; T_{h} is a dimensionless time factor for horizontal drainage; μ is a parameter representing the geometry of the vertical drain; $n = d_{\mathrm{e}}/d_{\mathrm{w}}$, where d_{e} is the diameter of the influence zone and d_{w} is the equivalent drain diameter of the vertical drain and can be calculated by $d_{\mathrm{w}} = 2(a + b)/\pi$ in which a and b are the width and thickness of the prefabricated vertical drain (PVD), respectively; $s = d_{\mathrm{s}}/d_{\mathrm{w}}$, where d_{s} is the smear diameter; k_{h} and k_{s} are the horizontal permeability coefficients in the undisturbed and smear zones, respectively; q_{w} is the well discharge capacity; and the subscripts "ax" and "s" denote axisymmetric conditions and the smear zone, respectively.

Plane strain condition

The governing equation for conventional radial consolidation is as follows:

$$[3] \qquad c_{\mathrm{h}}\frac{\partial^2 u}{\partial x^2}=\frac{\partial u}{\partial t}$$

The solution for this equation (modified after Indraratna and Redana 2000) is given by

$$[4a] \qquad \frac{\bar{u}}{\sigma_1}=\exp\left(\frac{-8T_{\mathrm{h,ps}}}{\mu_{\mathrm{ps}}}\right)$$

where

$$[4b] \qquad \mu_{\mathrm{ps}}=\left(\alpha+\frac{k_{\mathrm{h,ps}}}{k_{\mathrm{s,ps}}}\beta+\theta\right)$$

where

$$\alpha=\frac{2}{3}\frac{(n-s)^3}{n^2(n-1)}$$

$$\beta=\frac{2(s-1)}{n^2(n-1)}\left[n(n-s-1)+\frac{1}{3}(s^2+s+1)\right]$$

and

$$\theta=\frac{4k_{\mathrm{h,ps}}}{3Bq_{\mathrm{w,ps}}}\left(1-\frac{1}{n}\right)l^2$$

$$[4c] \qquad T_{\mathrm{h,ps}}=c_{\mathrm{h,ps}}t/B^2$$

where $n = B/b_{\mathrm{w}}$; $s = b_{\mathrm{s}}/b_{\mathrm{w}}$; α is the geometric parameter representing the influence zone; β is the geometric parameter representing the smear effect; θ is the geometric parameter representing the well resistance; and the subscript "ps" denotes the plane strain condition. For plane strain analysis, B, b_{s}, and b_{w} are assumed to be equal to r_{e} (radius of influence zone), r_{s} (radius of smear zone), and r_{w} (radius of drain well), respectively (also refer to Fig. 1).

Analytical model for a vertical drain with vacuum preloading

Experience has shown that when vacuum pressure is applied in the field through PVDs, the suction head along the drain length may decrease with depth, thereby reducing the efficiency (Chu et al. 2000). In the case of short vertical drains, laboratory measurements at a few points along the drain in the large-scale consolidometer (Fig. 2*a*) clearly indicated that the vacuum pressure not only propagates immediately but also decreases down the drain length. The rate of development of vacuum pressure within the drain may depend on the length and type of PVD (core and filter properties), but some field studies suggest that the vacuum pressure develops rapidly even if the PVDs are long (Bo et al. 2003). To study the effect of vacuum loss, the vacuum pressure distribution along the drain boundary is considered to vary linearly from $-p_0$ at the top of the drain to $-k_1p_0$ at the bottom of the drain, where k_1 is the ratio between the vacuum pressure at the bottom of the drain and that at the top of the drain (Fig. 2*b*)

Solution for the axisymmetric condition

The flow rate in the radial direction in the unit cell can be expressed by Darcy's law as

Fig. 2. (*a*) Distributions of measured negative pore-water pressure along drain boundary in laboratory testing. (*b*) Distributions of vacuum pressure in analytical model. (*c*) Vertical cross section of unit cell showing flow condition in vertical drain.

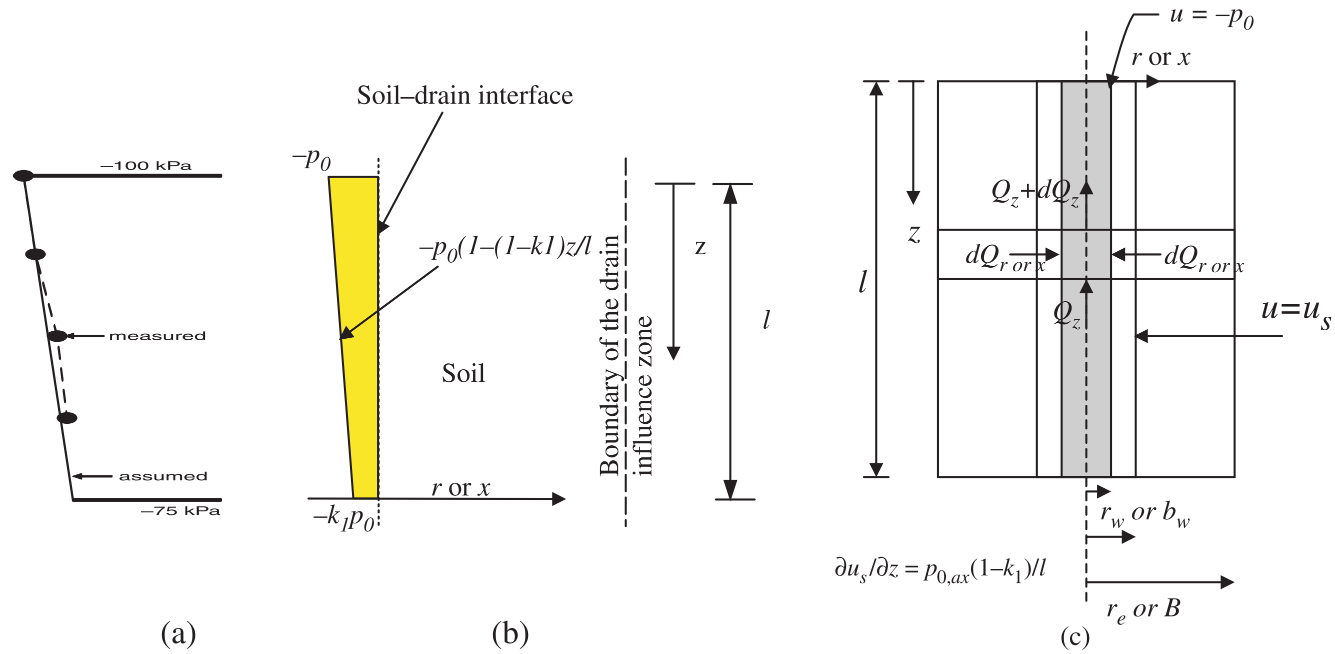

$$\frac{\partial Q}{\partial t} = \frac{k}{\gamma_w}\frac{\partial u}{\partial r}A \tag{5}$$

where Q is the flow in the soil mass, u is the excess pore pressure due to preloading, A is the cross-sectional area of the flow at distance r and is equal to $2\pi r\, dz$, γ_w is the unit weight of water, and k is the permeability coefficient of soil.

The rate of change in volume of the soil mass in the vertical direction is given by

$$\frac{\partial V}{\partial t} = \frac{\partial \varepsilon}{\partial t}\pi(r_e^2 - r^2)\, dz \tag{6}$$

where V is the volume of the soil mass, and ε is the vertical strain.

The radial flow rate in the unit cell is assumed to be equal to the rate of volume change of the soil mass in the vertical direction, therefore

$$\frac{k}{\gamma_w}\frac{\partial u}{\partial r}2\pi r(dz) = \frac{\partial \varepsilon}{\partial t}\pi(r_e^2 - r^2)\, dz \tag{7}$$

By rearranging eq. (7), the excess pore pressure gradient outside the smear zone can be derived as

$$\frac{\partial u}{\partial r} = \frac{\gamma_w}{2k_{h,ax}}\frac{\partial \varepsilon}{\partial t}\left(\frac{r_e^2 - r^2}{r}\right) \qquad \text{for } r_s \le r \le r_e \tag{8}$$

Similarly, in the smear zone, the corresponding pore pressure gradient is given by

$$\frac{\partial u_s}{\partial r} = \frac{\gamma_w}{2k_{s,ax}}\frac{\partial \varepsilon}{\partial t}\left(\frac{r_e^2 - r^2}{r}\right) \qquad \text{for } r_w \le r \le r_s \tag{9}$$

Considering the horizontal cross-sectional slice of thickness dz of a circular cylindrical drain with radius r_w (Fig. 2*c*), the change of flow in the z direction of the drain from the entrance to the exit of the slice dQ_z is expressed by

$$dQ_z = \frac{q_w}{\gamma_w}\frac{\partial^2 u}{\partial z^2}\, dz\, dt \qquad \text{for } r \le r_w \tag{10}$$

where the flow term q_w represents well resistance. Unless the drains are very large (>20 m), twisted, or folded, the well resistance of most PVDs can generally be neglected (Holtz et al. 1991; Indraratna and Redana 2000).

The total change in flow from the entrance face to the exit face of the slice is given by

$$dQ_r = \frac{2\pi r_w k_{s,ax}}{\gamma_w}\frac{\partial u}{\partial r}\, dz\, dt \qquad \text{for } r = r_w \tag{11}$$

If the water is assumed to be incompressible, the following equation should be satisfied:

$$dQ_z + dQ_r = 0 \tag{12}$$

At the drain boundary ($r = r_w$), it is assumed that a sudden drop in pore pressure does not take place, hence $u = u_s$, where u_s is the excess pore pressure in the smear zone. Substituting eqs. [10] and [11] in eq. [12] and subsequent rearranging with the aforementioned boundary conditions yields

$$\left(\frac{\partial u_s}{\partial r}\right)_{r=r_w} + \frac{q_w}{2\pi r_w k_{s,ax}}\left(\frac{\partial^2 u_s}{\partial z^2}\right)_{r=r_w} = 0 \tag{13}$$

Integrating eq. [13] in the z direction (after substituting eq. [9] into eq. [13] and subject to the boundary conditions (*i*) at $z = 0$, $u_s = -p_{0,ax}$ (applied vacuum pressure), and (*ii*) at $z = l$, $\partial u_s/\partial z = p_{0,ax}(1 - k_1)/l$), the excess pore pressure at $r = r_w$ can be determined by

$$[14]\quad (u_s)_{r=r_w} = -p_{0,ax}\left[1-(1-k_1)\frac{z}{l}\right] + \frac{\gamma_w \pi r_w^2}{q_w}\frac{\partial \varepsilon}{\partial t}(n^2-1)\left(lz-\frac{z^2}{2}\right)$$

Integrating eqs. [8] and [9] in the r direction with the boundary conditions given in eq. [14], and by assuming $u_s = u$ at the interface $r = r_s$ (see Fig. 2c), u_s and u can be expressed by

$$[15]\quad u_s = -p_{0,ax}\left[1-(1-k_1)\frac{z}{l}\right] + \frac{\gamma_w}{2k_{s,ax}}\frac{\partial \varepsilon}{\partial t} \times \left[r_e^2 \ln\frac{r}{r_w} - \frac{r^2-r_w^2}{2} + \frac{\pi r_w^2 k_{s,ax}}{q_w}(n^2-1)(2lz-z^2)\right] \quad \text{for } r_w \le r \le r_s$$

$$[16]\quad u = -p_{0,ax}\left[1-(1-k_1)\frac{z}{l}\right] + \frac{\gamma_w}{2k_{h,ax}}\frac{\partial \varepsilon}{\partial t} \times \left[r_e^2 \ln\frac{r}{r_s} - \frac{r^2-r_s^2}{2} + \frac{k_{h,ax}}{k_{s,ax}}\left(r_e^2 \ln s - \frac{r_s^2-r^2}{2}\right) + \frac{\pi r_w^2 k_{h,ax}}{q_w}(n^2-1)(2lz-z^2)\right] \quad \text{for } r_s \le r \le r_e$$

The mean excess pore pressure ($\bar{u}$) is determined from

$$[17]\quad \bar{u}\pi(r_e^2-r_w^2)l = \int_0^l\int_{r_w}^{r_s} 2\pi u_s r\,\mathrm{d}r\,\mathrm{d}z + \int_0^l\int_{r_s}^{r_e} 2\pi u r\,\mathrm{d}r\,\mathrm{d}z$$

Integrating eq. [17] after substitution of eqs. [15] and [16], the average excess pore pressure is given by

$$[18]\quad \bar{u} = \frac{\gamma_w}{2k_{h,ax}}\frac{\partial \varepsilon}{\partial t}\frac{d_e^2}{4}\mu_{ax} - \frac{(1+k_1)p_{0,ax}}{2}$$

where

$$\mu_{ax} = \frac{n^2}{n^2-1}\left[\ln\left(\frac{n}{s}\right) + \frac{k_{h,ax}}{k_{s,ax}}\ln(s) - \frac{3}{4}\right] + \frac{s^2}{n^2-1} \times \left(1-\frac{s^2}{4n^2}\right) + \frac{k_{h,ax}}{k_{s,ax}}\frac{1}{n^2-1}\left(\frac{s^4-1}{4n^2} - s^2 + 1\right) + \pi\frac{2k_{h,ax}}{3q_w}l^2\left(1-\frac{1}{n^2}\right)$$
$$\approx \left[\ln\left(\frac{n}{s}\right) + \frac{k_{h,ax}}{k_{s,ax}}\ln(s) - \frac{3}{4} + \pi\frac{2k_{h,ax}}{3q_w}l^2\right]$$

If the well resistance is ignored, μ_{ax} becomes

$$\mu_{ax} \approx \left[\ln\left(\frac{n}{s}\right) + \frac{k_{h,ax}}{k_{s,ax}}\ln(s) - \frac{3}{4}\right]$$

If the well resistance and smear effect are ignored, μ_{ax} becomes

$$\mu_{ax} \approx \left[\ln(n) - \frac{3}{4}\right]$$

Combining eq. [18] with the well-known compressibility relationship $\partial\varepsilon/\partial t = -m_v\,\partial\bar{u}/\partial t$ gives

$$[19]\quad \bar{u} = -\frac{\gamma_w}{8k_{h,ax}}m_v\frac{\partial \bar{u}}{\partial t}d_e^2\mu_{ax} - \frac{(1+k_1)p_{0,ax}}{2}$$

where m_v is the coefficient of volume compressibility for one-dimensional compression. Rearranging eq. [19] and then integrating by applying the boundary condition $\bar{u} = \sigma_1$ at t = 0 gives

$$[20]\quad \frac{\bar{u}}{\sigma_1} = \left[1+\frac{(1+k_1)p_{0,ax}}{2\sigma_1}\right]\exp\left(\frac{-8T_{h,ax}}{\mu_{ax}}\right) - \frac{(1+k_1)p_{0,ax}}{2\sigma_1}$$

For eq. [20], the vacuum pressure ratio (VPR) can be introduced by the value of p_0/σ_1 (i.e., (applied vacuum pressure)/(preloading pressure)).

The average degree of consolidation (U_h in %) can now be evaluated conveniently by the following equation:

$$[21]\quad U_h = \frac{1-\bar{u}/\sigma_1}{1-\bar{u}_\infty/\sigma_1}\times 100$$

where $\bar{u}_\infty/\sigma_1$ can be calculated by eq. [20] when $t \to \infty$, and $\bar{u}_\infty$ is the average applied vacuum pressure for the unit cell.

For long drains, if the vacuum pressure at the bottom of the drain is assumed to be zero (i.e., k_1 = 0), eq. [20] becomes

$$[22]\quad \frac{\bar{u}}{\sigma_1} = \left(1+\frac{p_{0,ax}}{2\sigma_1}\right)\exp\left(\frac{-8T_{h,ax}}{\mu_{ax}}\right) - \frac{p_{0,ax}}{2\sigma_1}$$

Solutions for the plane strain condition

Since the procedures for plane strain analysis are similar to those for the axisymmetric condition, the exact solution can be written as follows (details are given in Appendix A):

$$[23]\quad \frac{\bar{u}}{\sigma_1} = \left[1+p_{0,ps}\frac{(1+k_1)}{2\sigma_1}\right]\exp\left(\frac{-8T_{h,ps}}{\mu_{ps}}\right) - \frac{p_{0,ps}}{\sigma_1}\frac{(1+k_1)}{2}$$

where

$$\mu_{ps} = \left[\alpha + \frac{k_{h,ps}}{k_{s,ps}}(\beta) + \theta\right] \qquad \alpha = \frac{2}{3}\frac{(n-s)^3}{n^2(n-1)}$$

$$\beta = \frac{2(s-1)}{n^2(n-1)}\left[n(n-s-1) + \frac{1}{3}(s^2+s+1)\right]$$

and

$$\theta = \frac{4k_{h,ps}}{3Bq_{w,ps}}\left(1-\frac{1}{n}\right)l^2$$

Neglecting the well resistance, μ_{ps} becomes

$$\mu_{ps} = \left[\alpha + \frac{k_{h,ps}}{k_{s,ps}}(\beta)\right]$$

Neglecting both well resistance and the smear effect, μ_{ps} becomes

$$\mu_{ps} = \frac{2}{3}\frac{(n-1)^2}{n^2}$$

When the vacuum pressure is zero at the bottom of the drain ($k_1 = 0$), the exact solution can be expressed by

$$[24] \quad \frac{\bar{u}}{\sigma_1} = \left(1 + \frac{p_{0,ps}}{2\sigma_1}\right)\exp\left(\frac{-8T_{h,ps}}{\mu_{ps}}\right) - \frac{p_{0,ps}}{2\sigma_1}$$

Numerical modeling of a vertical drain incorporating vacuum preloading

The finite element program ABAQUS was used to simulate the unit cell of a vertical drain, where an elastic analysis was conducted with $m_v = 10^{-3}$ m^2/kN and with Poisson's ratio $\nu = 0$ to simulate the condition of zero lateral displacement. The consolidation analysis based on Biot's solution is used in ABAQUS. In the field, at the embankment centreline (exploiting symmetry), the condition of negligible lateral displacement can be justified. A reconstituted clay from Sydney, Australia, was used to conduct large-scale consolidation testing to measure the vacuum pressure distribution along the drain. The soil properties were examined using the same large-scale consolidation tests and have been described by Indraratna and Redana (1997). The horizontal undisturbed soil permeability ($k_{h,ax}$) was determined from one-dimensional (1D) consolidation tests to be approximately 10^{-10} m/s. According to Indraratna and Redana (2000), the ratio of the undisturbed permeability to the smear zone permeability ($k_{h,ax}/k_{s,ax}$) was assumed to be 3.0. The top, bottom, and outer boundaries were set as impermeable (see Fig. 3*b*). The vertical loading pressure (σ_1 = 50 kPa) was applied at the top of the cell. The horizontal displacement boundary was fixed (i.e., no movement in the horizontal direction), and vertical displacement was permitted. A VPR of unity was employed (i.e., $p_0/\sigma_1 = 1.0$). To avoid non-uniform settlement (equal strain condition), rigid elements were selected at the soil surface. For the analytical and numerical analysis, the following two cases were examined.

Case A: short-drain analysis — The dimensions of the unit cell (see Fig. 3) were 450 mm (i.e., influence zone diameter or the width of the unit cell) and 950 mm (height). The equivalent drain diameter (d_w) or drain width ($2b_w$) was taken to be 50 mm. The smear diameter (d_s) or smear zone width ($2b_s$) was 170 mm, based on laboratory testing by Indraratna and Redana (1997). A total of 160 elements (eight-node biquadratic displacement and bilinear pore pressure) were used in the finite element analysis (Figs. 3*a*, 3*b*). In the entire finite element mesh, the aspect ratio of elements was kept below 3. To simulate the drain boundary, the pore pressure was either set to zero for the conventional case (no vacuum pressure) or specified to be maximum (negative) at the top, reducing linearly to 75% of applied vacuum pressure at the bottom (k_1 = 0.75), in agreement with the laboratory results shown in Fig. 2*a*.

Case B: long-drain analysis — The dimensions of the unit cell and vertical drain were kept the same as those in case A. To simulate a long vertical drain, the height of soil was taken to be 10 m, and the vacuum pressure at the bottom of the drain was assumed to be zero. The pore pressure at the drain boundary was set to maximum ($-p_0$) at the top, reducing linearly to zero at the bottom (Fig. 3*c*).

Validation of the finite element model (FEM) incorporating the analytical solutions

The analytical solutions developed by the authors including the equivalent plane strain parameters can be readily input via appropriate subroutines in commercial software such as ABAQUS. The results of a finite element (ABAQUS) analysis with and without smear effects are plotted together with the analytical predictions in the form of average excess pore pressure ratios and time. Negligible error between these plots verifies the validity of the FEM capturing the authors' solution. The predicted average excess pore pressure is calculated using the excess pore pressure values obtained from the finite element analysis. In the following analysis, the discharge capacity (q_w) of the drain is assumed to be high enough for well resistance to be neglected. Indraratna and Redana (2000) described that well resistance becomes significant for PVD with q_w less than 40–60 m^3/year. First, the results of numerical modeling of a vertical drain without vacuum pressure are validated with the analytical model. Second, the analytical and numerical solutions with vacuum pressure are validated.

Vertical drain without vacuum preloading

A comparison of the average excess pore-water pressure ratio ($\bar{u}/\sigma_1$) from the analytical model (eq. [2]) and numerical predictions for the axisymmetric condition is shown in Fig. 4. For this study, a c_h value of 0.32 m^2/year obtained from a 1D consolidation test and an r_e value of 225 mm were used for the relationship between time factor (T_h) and time (t), and a good agreement was found. Very small deviations are noted for the range $30 < t < 200$ days ($0.13 < T_h < 0.84$), with a maximum error of about 4%. Figure 5 illustrates the comparison of average excess pore pressure ratio between the analytical model (eq. [4]) and the numerical solution for the plane strain condition. Again, there was good agreement between the two models, with the difference in results becoming insignificant for $t > 10$ days ($T_h > 0.04$).

Vertical drain with vacuum preloading

Figures 6 and 7 compare the average excess pore pressure ratio for cases A and B for axisymmetric and plane strain conditions, respectively. For axisymmetric conditions, the results from the finite element and analytical models (eq. [20] for case A and eq. [22] for case B) are in good agreement (Fig. 6). For plane strain conditions (Fig. 7), the results from the analytical solution (i.e., eq. [23] for case A and eq. [24] for case B) agree well with those from the numerical solutions for the entire range of time, with the maximum deviation observed around 10 days for the smear effect (i.e., $T_h \approx 0.04$). For axisymmetric conditions (Fig. 6), the difference in

Fig. 3. Finite element discretization for axisymmetric and plane strain analyses of soil in unit cell: (*a*) nodes and integration points for a single eight-node biquadratic displacement, bilinear pore pressure element; (*b*) mesh discretization and vacuum pressure distribution for short-drain analysis (case A; not to scale); (*c*) mesh discretization and vacuum pressure distribution for long-drain analysis (case B; not to scale).

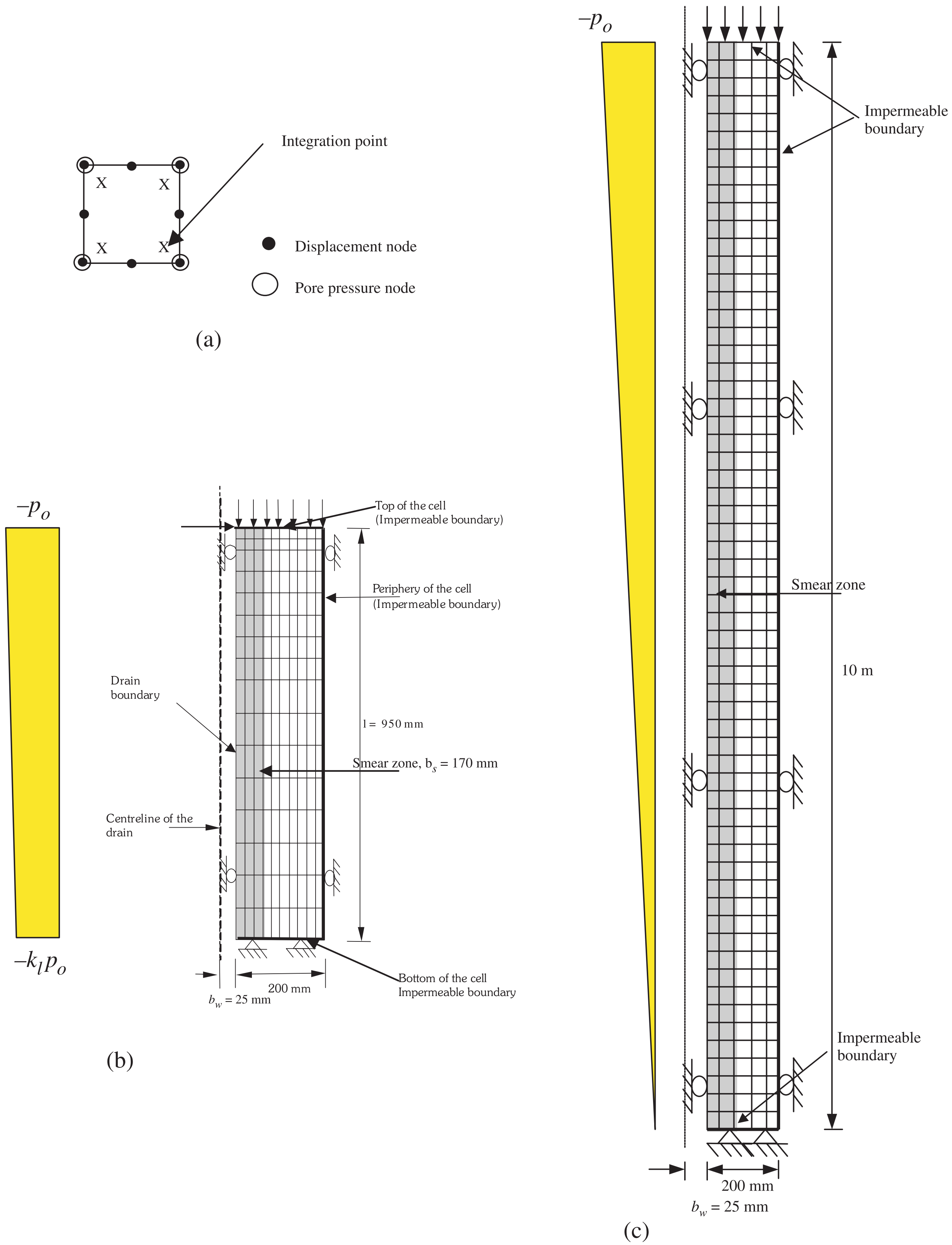

Fig. 4. Finite element (FEM) and analytical model results for axisymmetric condition.

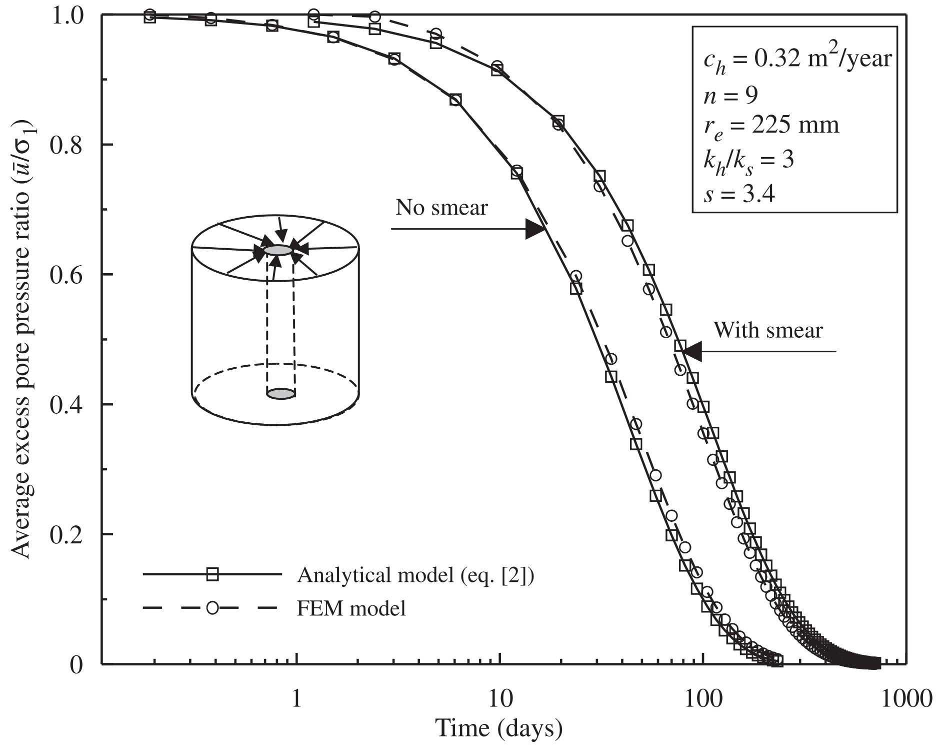

average excess pore pressure ratio between case A (25% vacuum loss with depth) and case B (vacuum pressure linearly decreasing with depth to zero at the bottom of the drain) becomes considerable after about 90 and 30 days for a drain with and without smear, respectively, when the average excess pore pressures of case A start to become negative. For the plane strain condition (Fig. 7), the deviation between case A and case B is significant after 30 days (with smear) and 20 days (ideal drain), where the average excess pore pressure ratio for case B is less negative compared with that for case A. Figures 6 and 7 confirm that the ultimate negative average excess pore pressure ratio for case A (approximately 0.90) is markedly different from that of case B (0.50). As discussed later in the paper, this also corresponds to a greater ultimate settlement associated with case A as compared with case B.

Comparison between axisymmetric and equivalent plane strain analyses

In general, the conversion procedure used in vertical drain modeling (Hird et al. 1992; Indraratna and Redana 1997, 2000) is useful in transforming parameters from the true axisymmetric condition (3D) to the equivalent plane strain condition conveniently employed in 2D finite element analyses. In this section, only the smear effect is considered in the analysis. The differences between the axisymmetric and plane strain conditions (prior to conversion) with and without vacuum preloading are shown in Figs. 8 and 9, respectively. For the conventional surcharge loading with no vacuum pressure (Fig. 8), the comparison between the axisymmetric and plane strain conditions confirms that the dissipation of average excess pore pressure is slower for the axisymmetric conditions than for the plane strain conditions. This is because the flow contact area of a drain wall in the unit cell is greater than that of a drain well as shown in Fig. 1. Figure 8 also shows that the final average excess pore pressure becomes zero after 200 days ($T_h \approx 0.8$) for plane strain but after 500 days for axisymmetric conditions ($T_h \approx 2.14$). Figures 9*a* and 9*b* illustrate the effect of different vacuum pressure distributions (cases A and B), where the plane strain model gives the greater dissipation of average excess pore pressure in comparison with the axisymmetric condition at any given time. As expected, the 25% vacuum loss along the drain (case A) shows a greater average excess pore pressure dissipation rate than the 100% vacuum loss along the drain (case B).

Figures 8 and 9 demonstrate that the axisymmetric and plane strain solutions cannot produce the same consolidation response. Therefore, to use a plane strain solution for vertical drains and still obtain the same consolidation as in the case of the true axisymmetric condition, one must employ a conversion procedure to derive an equivalent plane strain solution that provides a very good match to the axisymmetric consolidation curve. An equivalent plane strain solution can be obtained by geometric transformation or permeability transformation or both to minimize the disparity between the two methods (Hird et al. 1992; Indraratna and Redana 1997, 2000). For vacuum preloading, the proposed "conversion" procedures can be based on the equivalent average excess pore pressure and the equivalent vacuum pressure by still maintaining the geometric equivalence (i.e., $d_w = 2b_w$, $d_s = 2b_s$, $d_e = 2B$ in Fig. 1). In this study, permeability and vacuum pressure relationships between the axisymmetric and

Fig. 5. Finite element and analytical model results for plane strain condition.

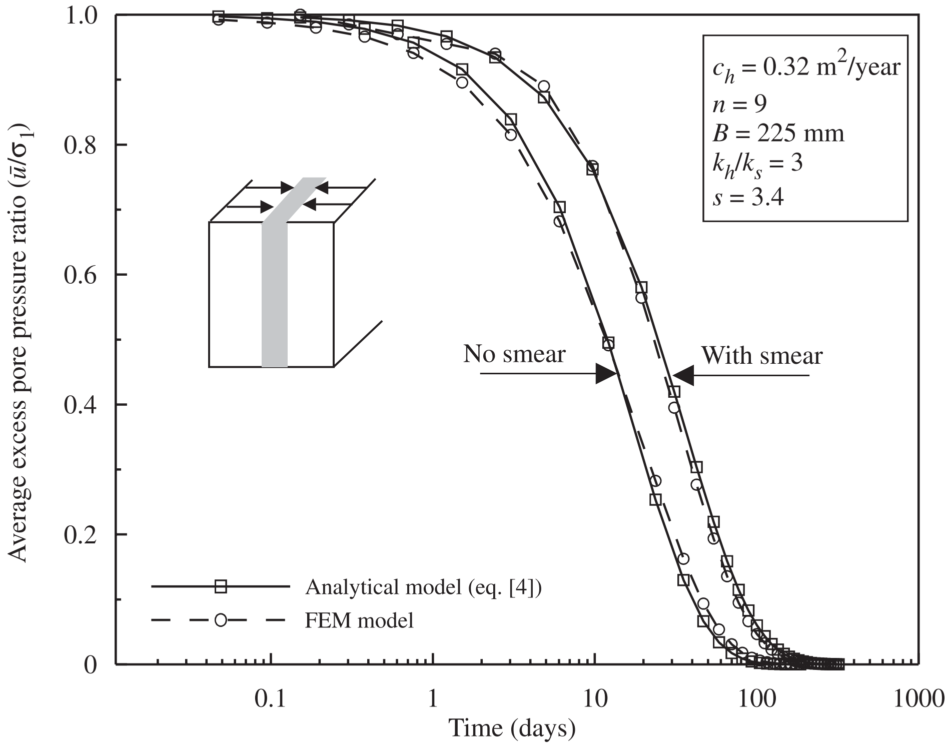

Fig. 6. Finite element and analytical model results (axisymmetric with vacuum preloading): (*a*) case A, short-drain analysis; (*b*) case B, long-drain analysis.

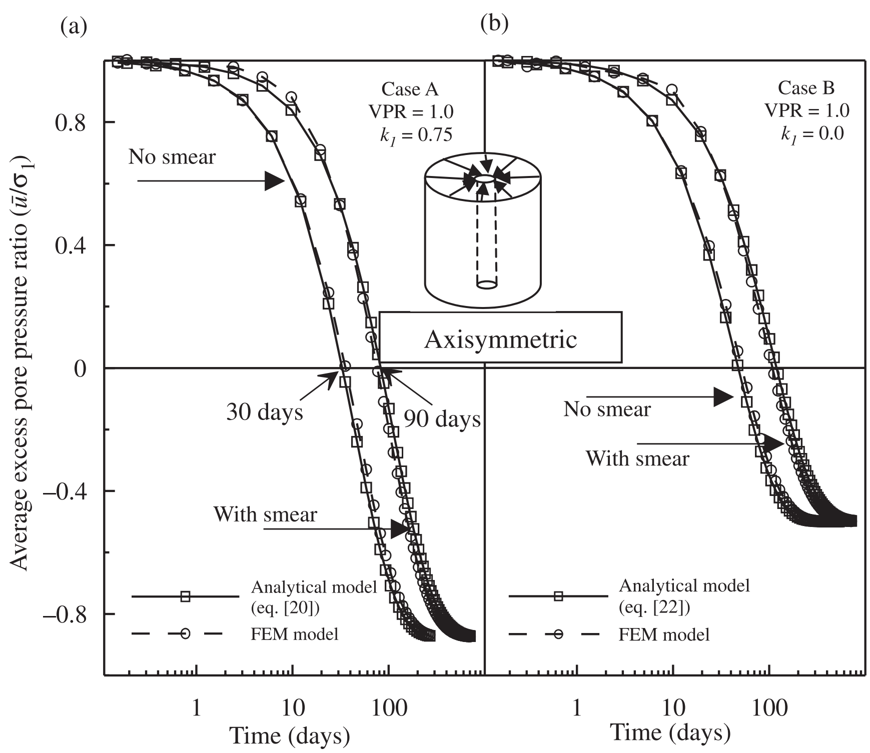

Fig. 7. Finite element and analytical model results (plane strain with vacuum preloading): (*a*) case A, short-drain analysis; (*b*) case B, long-drain analysis.

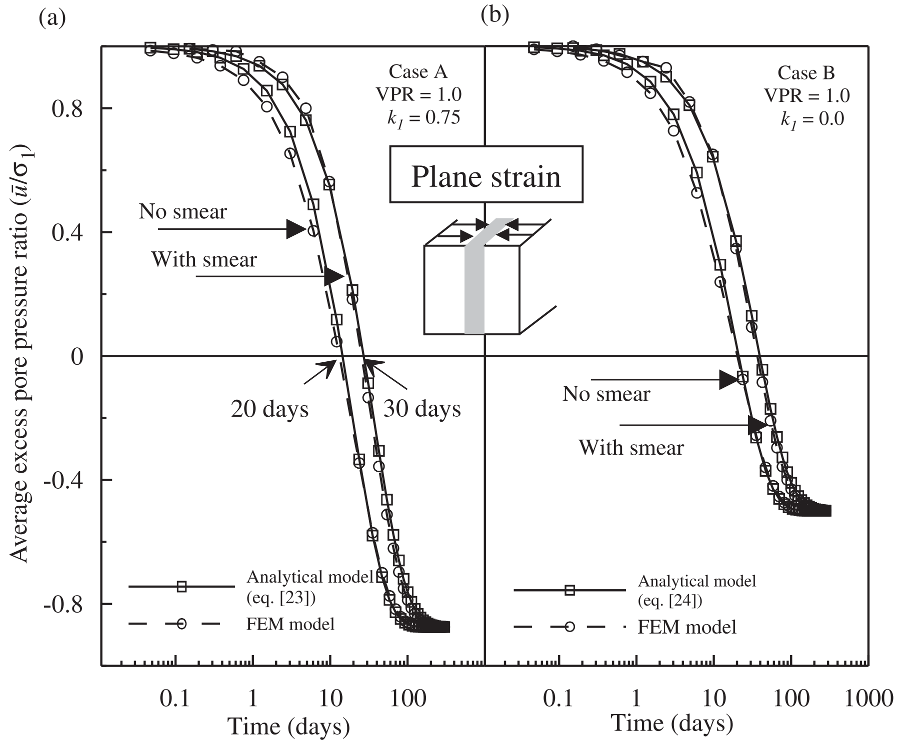

Fig. 8. Difference between original axisymmetric and plane strain analyses prior to establishing the equivalent plane strain conversion with smear effect.

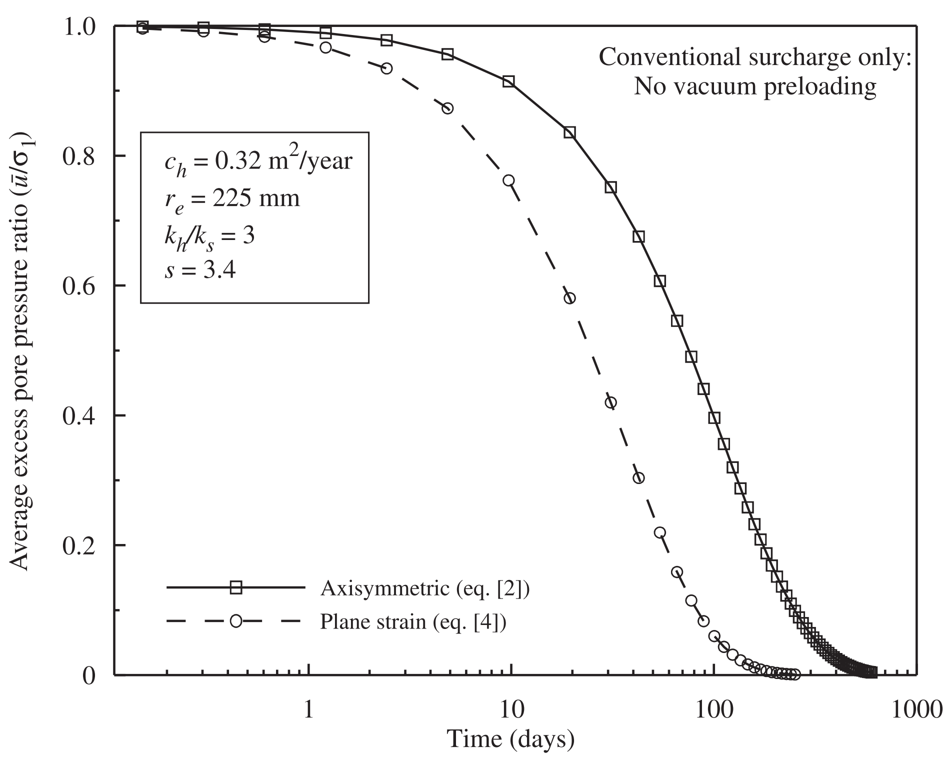

Fig. 9. Difference between axisymmetric and plane strain analyses prior to establishing the equivalent plane strain conversion: (*a*) case A, short drain; (*b*) case B, long drain.

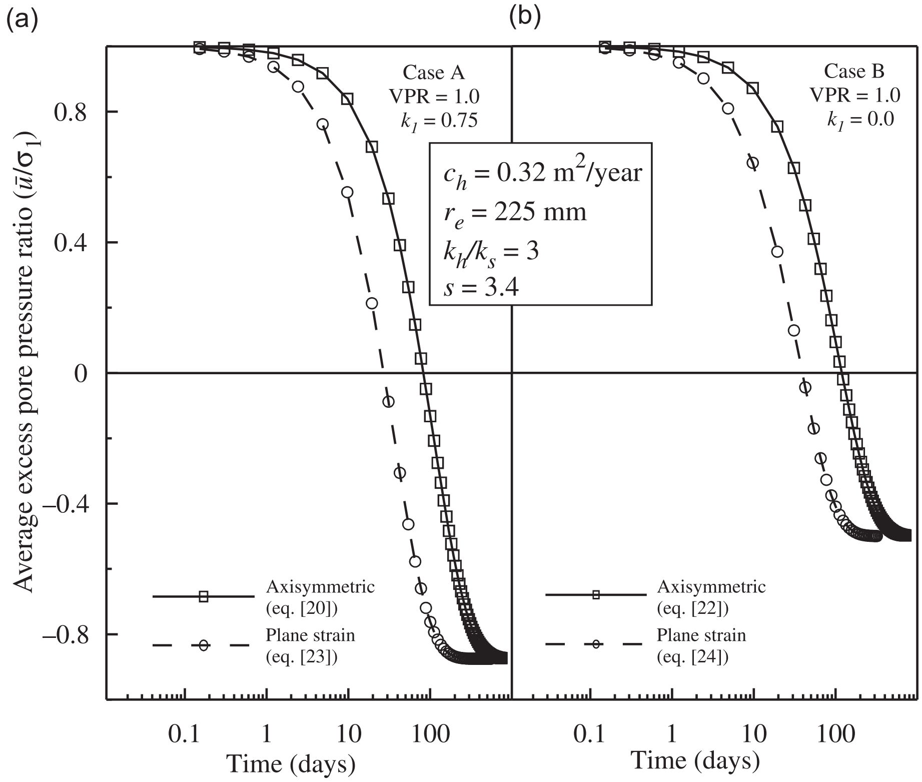

equivalent plane strain conditions have been derived by extending the previous theory developed by Indraratna and Redana (1997) and are explained in the following.

At a given stress level and at each time step, the average excess pore pressures for both axisymmetric and plane strain conditions are made equal by equating eq. [20] with eq. [23]. The equivalent permeability and equivalent applied vacuum pressure for the equivalent plane strain condition can now be expressed in the following.

The equivalent permeability under plane strain is given by

$$[25] \quad \frac{k_{\mathrm{h,ps}}}{k_{\mathrm{h,ax}}} = \frac{\left[\alpha + \dfrac{k_{\mathrm{h,ps}}}{k_{\mathrm{s,ps}}}(\beta) + \theta\right]}{\left[\ln\left(\dfrac{\mathrm{n}}{\mathrm{s}}\right) + \dfrac{k_{\mathrm{h,ax}}}{k_{\mathrm{s,ax}}}\ln(s) - \dfrac{3}{4} + \pi\dfrac{2k_{\mathrm{h,ax}}}{3q_{\mathrm{w}}}l^2\right]}$$

Neglecting the well resistance in eq. [25], the ratio of the smear zone permeability to the undisturbed zone permeability is as follows:

$$[26] \quad \frac{k_{\mathrm{s,ps}}}{k_{\mathrm{h,ps}}} = \frac{\beta}{\dfrac{k_{\mathrm{h,ps}}}{k_{\mathrm{h,ax}}}\left[\ln\left(\dfrac{\mathrm{n}}{\mathrm{s}}\right) + \dfrac{k_{\mathrm{h,ax}}}{k_{\mathrm{s,ax}}}\ln(s) - \dfrac{3}{4}\right] - \alpha}$$

Ignoring both smear and well resistance effects, the simplified ratio of equivalent plane strain permeability to axisymmetric permeability in the undisturbed zone can be obtained:

$$[27] \quad \frac{k_{\mathrm{h,ps}}}{k_{\mathrm{h,ax}}} = \frac{\dfrac{2}{3}\dfrac{(n-1)^2}{n^2}}{[\ln(n) - 0.75]}$$

The equivalent vacuum pressure can be determined by

$$[28] \quad p_{0,\mathrm{ps}} = p_{0,\mathrm{ax}}$$

To examine the validity of the aforementioned conversion procedure, the analytical and numerical models were employed to compare the deviations between the axisymmetric and equivalent plane strain conditions. Based on eqs. [26]–[28], Table 1 shows the parameters used in the axisymmetric and equivalent plane strain conditions for both short- and long-drain analyses (i.e., cases A and B).

After conversion of the original plane strain condition to the equivalent plane strain condition, the results are identical, as shown in Figs. 10*a* and 10*b*. Figure 10*b* illustrates the corresponding finite element simulations, which also indicate very similar results. Comparison of Figs. 10*a* and 10*b* confirms that the results of finite element and analytical models almost coincide, and hence, for the purpose of clarity, the analytical and finite element results are plotted separately. Figure 11 compares the results of the analytical and numerical models after application of the permeability and vacuum pressure conversions for cases A and B. The analytical plane strain and analytical axisymmetric models give identical results, whereas the finite element models show a very small discrepancy. In general, the aforementioned matching procedure confirms the reliability of the equivalent plane strain model for both case A and case B.

Table 1. Permeability coefficient and vacuum pressure values for axisymmetric and equivalent plane strain conditions.

Conversion parameter	Axisymmetric	Equivalent plane strain	Equation No.
Undisturbed horizontal permeability, k_h ($\times 10^{-10}$ m/s)	1.00	0.36	27
Smear permeability, k_s ($\times 10^{-10}$ m/s)	0.33	0.10	26
Vacuum pressure (×100 kPa)	0.50	0.50	28

Fig. 10. Comparison of axisymmetric model with the equivalent plane strain model including smear effect: (*a*) analytical method; (*b*) FEM.

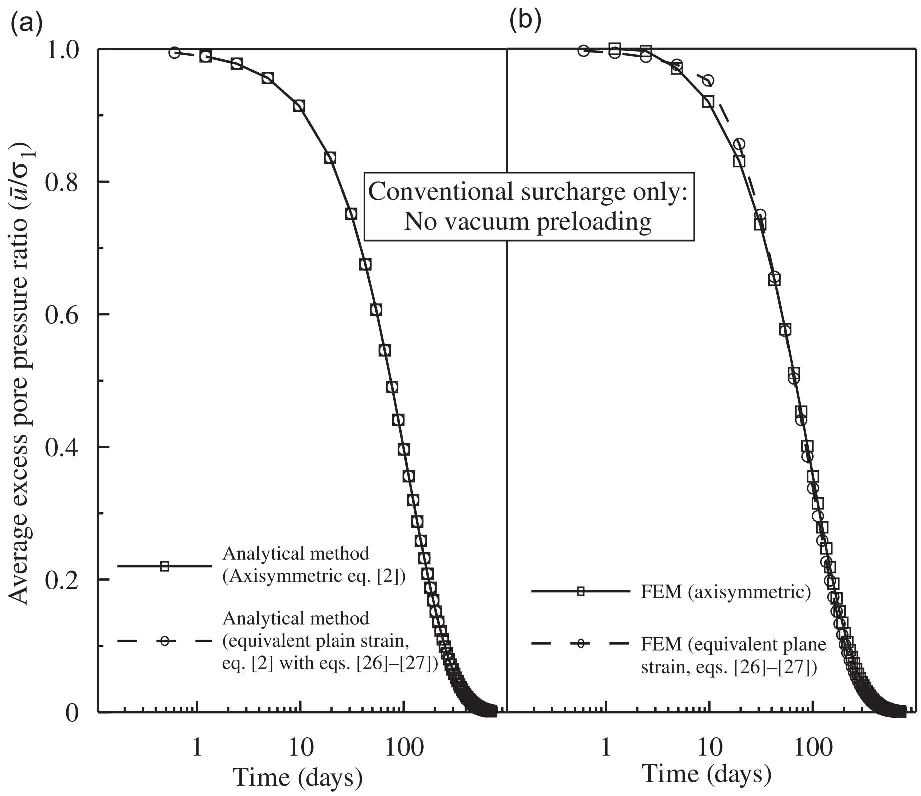

Effect of the magnitude and distribution of vacuum pressure

In this section, the effects of the magnitude and distribution of vacuum pressure along the vertical drain are discussed based on the equivalent plane strain condition. The comparison of settlement between analytical and numerical models with variation of VPR for cases A and B is shown in Figs. 12*a* and 12*b*, respectively (eqs. [23]–[28]). Almost identical results were found for the two approaches. As expected, the rate of settlement with applied vacuum pressure was faster than that with conventional loading (surcharge only) without vacuum pressure.

Figure 12 also shows that, at the higher VPR, the rate of settlement and the final settlement are increased. Clearly, the application of vacuum pressure increases the lateral pore pressure gradient, thus promoting radial flow. The accelerated consolidation increases the rate of settlement and the ultimate settlement, which is analogous to increasing the applied surcharge load. The consideration of varying vacuum pressure along the length of the drain is more realistic, as the effect of vacuum usually diminishes with an increase in depth. In other words, for long vertical drains, it is possible that the applied vacuum pressure at the drain top may not be propagated towards the bottom part of the drain. The results plotted in Fig. 12 show that the rate of consolidation for 25% vacuum loss (case A) is more rapid compared with that for case B. It is also clear that the greater the magnitude of the vacuum pressure ratio, the higher the rate of consolidation; however, unless the magnitude of the vacuum pressure is large enough (e.g., VPR > 0.25), the effect on excess pore pressure dissipation may not be significant in practice.

Practical implications

The effectiveness of a vertical drain incorporating vacuum pressure depends not only on the magnitude of the applied vacuum pressure but also on the vacuum pressure ratio. As mentioned previously, if the VPR is small (less than 0.25), the effect of vacuum preloading may not be significant. In the successful field applications, the applied vacuum pressure ratio has been as high as 1–2 (e.g., the Tianjin project (Chu et al. 2000) and the Yaoqiang Airport (Tang and Shang 2000)). With regard to the distribution of applied vacuum pressure, the almost constant vacuum pressure with depth may be used to predict the field behavior of short vertical

Fig. 11. Comparison of analytical and FEM solutions after conversion to equivalent plane strain condition including smear effect: (*a*) case A, analytical method; (*b*) case A, FEM; (*c*) case B, analytical method; (*d*) case B, FEM.

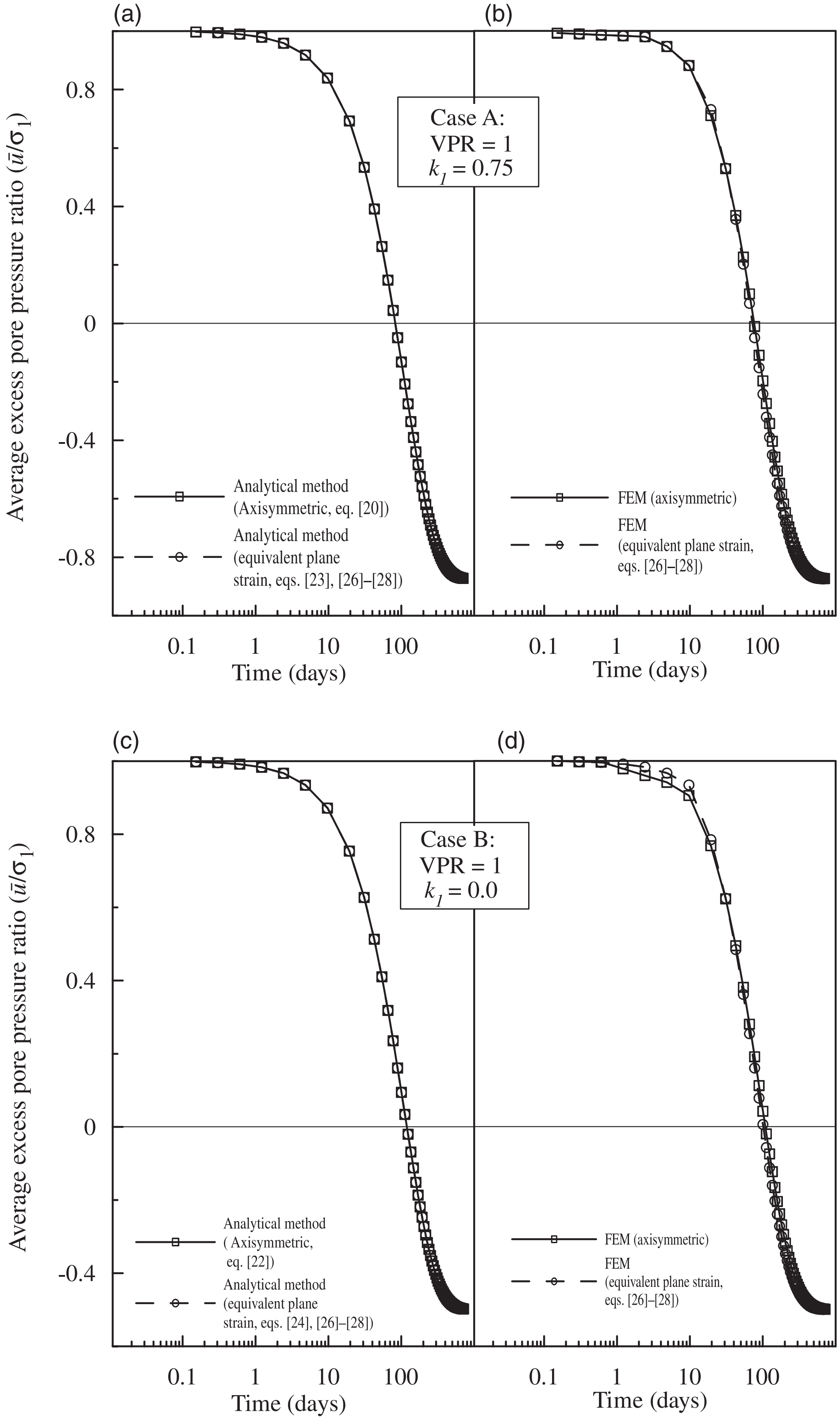

Fig. 12. Settlement results from analytical and FEM solutions after conversion to equivalent plane strain condition: (*a*) case A, short drain; (*b*) case B, long drain.

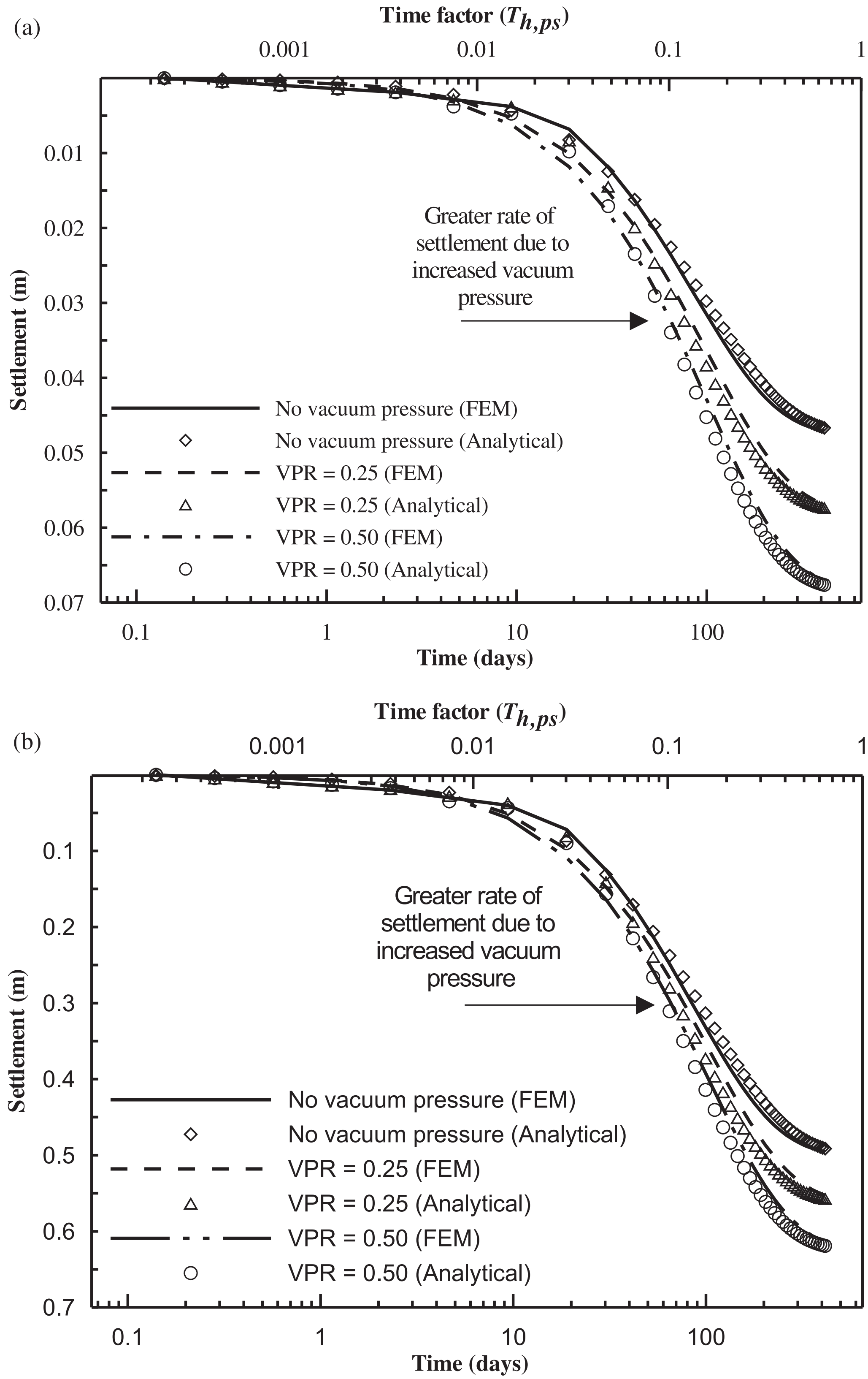

Fig. 13. Normalized settlement–time factor curves for varying *n* and VPR values based on the equivalent plane strain solution for ideal condition: (*a*) case A, short drain; (*b*) case B, long drain.

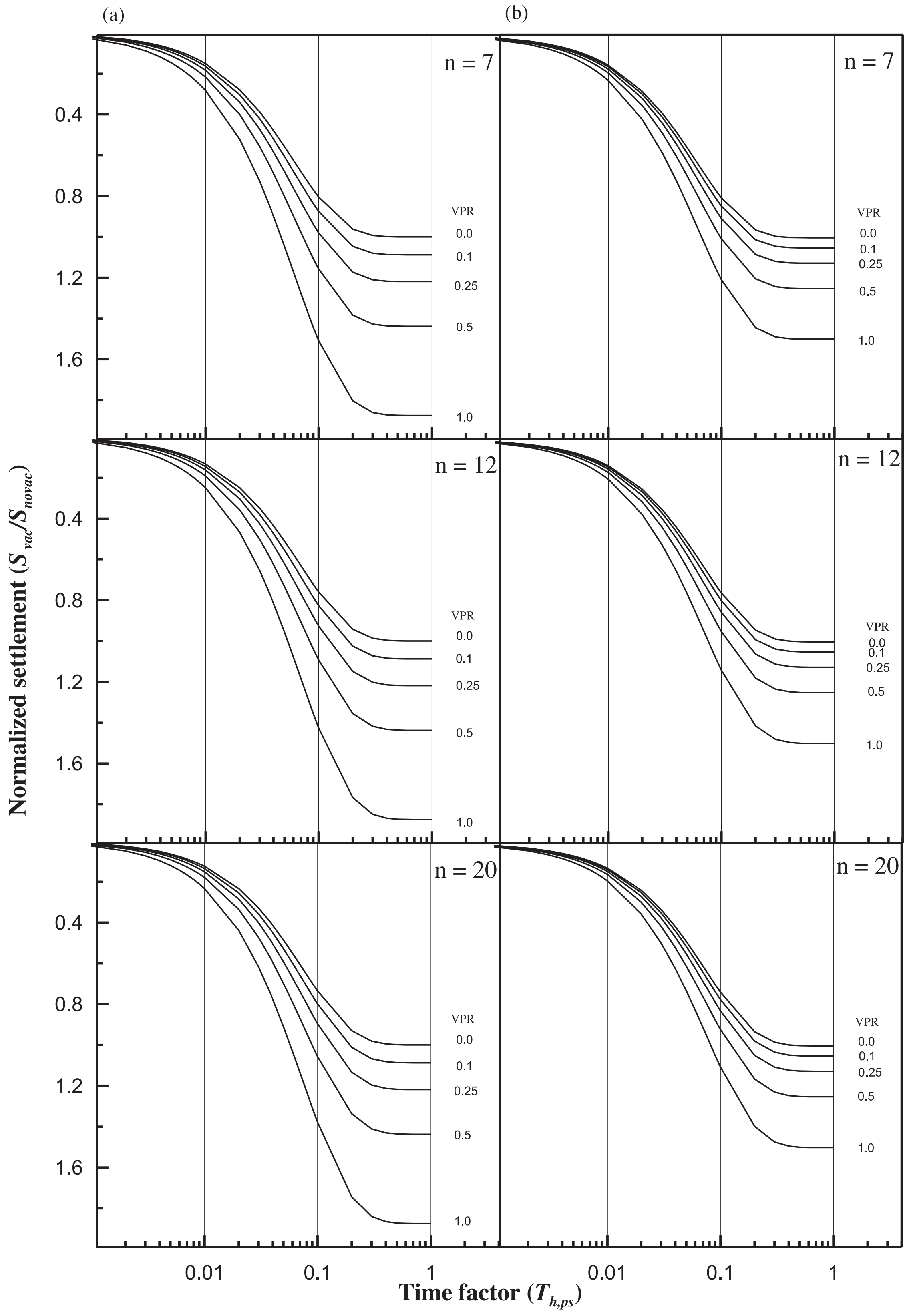

Fig. 14. Normalized settlement–time factor curves for varying n and VPR values based on the equivalent plane strain solution for s = 3 and k_h/k_s = 3: (a) case A, short drain; (b) case B, long drain.

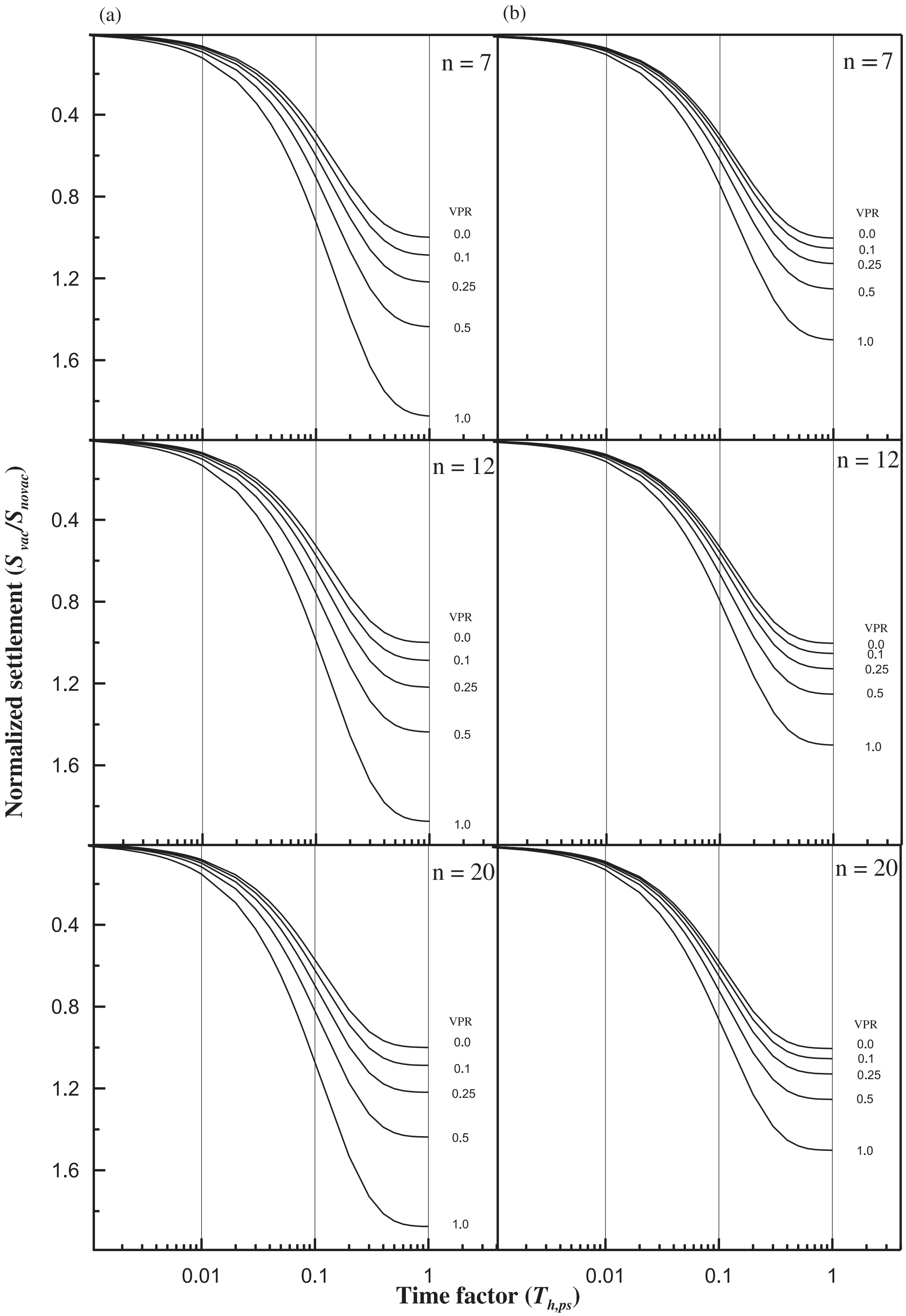

Fig. 15. Normalized settlement–time factor curves for varying n and VPR values based on the equivalent plane strain solution for s = 3 and k_h/k_s = 5: (a) case A, short drain; (b) case B, long drain.

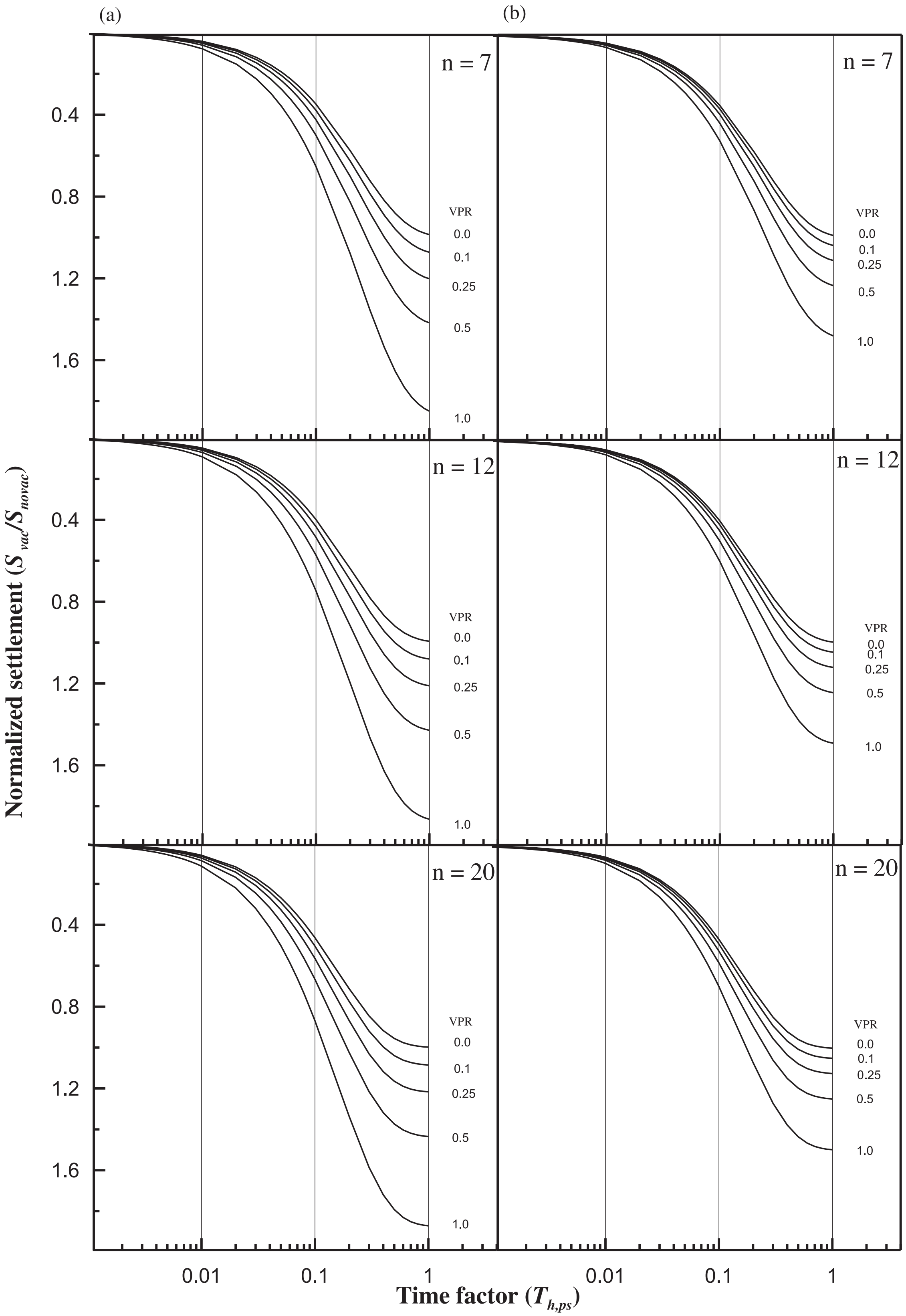

drains (say less than 10 m). In the case of long vertical drains (exceeding 10 m), Chu et al. (2000) demonstrated that by applying a vacuum pressure, the reduction in the excess pore-water pressure decreases with an increase in depth. This indicates that the diminishing vacuum pressure with depth (assumed linear) is a simplified and useful approach for predicting the performance of long vertical drains.

Most finite element analyses on soft clay embankments are conducted based on the 2D plane strain assumption. Although the consolidation around vertical drains is axisymmetric, in the case of multidrain analysis of large projects, plane strain analysis is certainly more efficient from a computational point of view when even the most sophisticated and powerful finite element codes fail to handle a large number of vertical drains, each having its own independent axisymmetric zone. Various researchers have described the advantages of such 2D plane strain solutions for field studies where a large number of drains are installed, for which a 3D analysis becomes cumbersome and often impractical (e.g., Hird et al. 1992; Chai et al. 1995; Indraratna et al. 1997; Bo et al. 2003).

Figure 13 illustrates the variation of the normalized settlement (S_{vac}/S_{novac}) versus time factor ($T_{h,ps}$) relationships with increasing VPR and n values for cases A and B (equivalent plane strain) for an ideal drain. The smear effect with a typical value of $s = 3$ and $k_h/k_s = 3$–5 is included in Figs. 14 and 15 based on the authors experience. Normalized settlement is defined as the ratio of settlement with vacuum pressure (S_{vac}) to the settlement without vacuum pressure (S_{novac}). Axisymmetric results are not plotted in Figs. 13–15 because they provide results almost identical to those of the equivalent plane strain condition. It is shown that unless the VPR values exceed 0.25, the additional consolidation due to the application of vacuum preloading may not be significant. In the field, VPR $\geq$ 1.0 and $n < 20$ will give considerably enhanced settlement (Tang and Shang 2000), as also supported by analytical results shown in Figs. 13–15. In summary, useful curves for normalized settlement for a given soil can be developed for an array of VPR and n values similar to the previous analysis, and these will be most beneficial for design engineers.

Conclusions

A system of vertical drains combined with vacuum preloading is an effective method for accelerating soil consolidation. In this study, an analytical model for a vertical drain (unit cell) incorporating vacuum preloading and smear and well resistance was developed for both axisymmetric and equivalent plane strain conditions. A finite element code (ABAQUS) was employed to analyze the unit cell and compare the numerical results with the writers' analytical approach. These comparisons confirmed the accuracy of the analytical formulations. A conversion procedure based on the transformation of permeability and vacuum pressure was also introduced to establish the relationships between the axisymmetric (3D) and equivalent plane strain (2D) conditions. Analytical and numerical schemes verified that the equivalent plane strain adaptation is as accurate as the conventional axisymmetric case, hence its adoption in practice can be justified.

In this paper, two different vacuum pressure distributions along a single drain were compared and discussed (i.e., for short and long drains). The simulation of varying vacuum pressure along the length of the drain is considered to be realistic because the applied vacuum pressure at the drain top may not always propagate towards the bottom part of the drain. In the field, this is probably true for the majority of long prefabricated vertical drains installed in soft clay, as indicated by past field studies. In the case of relatively short vertical drains (say less than 10 m), however, the approximation of constant vacuum pressure with depth may be justified. In practice, the effectiveness of vacuum preloading in soft clay depends on the magnitude of the applied vacuum pressure ratio and its actual distribution along the drain length. It is noted from the findings of this study that, if the vacuum pressure ratio (VPR) is less than 0.25, the effect of vacuum preloading on the excess pore pressure dissipation, and hence additional settlement, is not significant. Moreover, for the same VPR, the rate of settlement in the case of short drains is greater than that in the case of long drains. Lastly, a typical chart was plotted of normalized settlement against time factor for various VPR and n values and provides a useful preliminary design guide for practicing engineers. Such charts may be produced for an array of VPR and n values, for either constant or varying vacuum pressure distributions with depth.

References

ABAQUS, Inc. 2004. ABAQUS/standard user's manual. ABAQUS, Inc., Providence, R.I.

Barron, R.A. 1948. Consolidation of fine-grained soils by drain wells. ASCE Transactions, **113**: 718–754.

Bo, M.W., Chu, J., Low, B.K., and Choa, V. 2003. Soil improvement; prefabricated vertical drain techniques. Thomson Learning, Singapore. 341 pp.

Chai, J.C., Miura, N., Sakajo, S., and Bergado, D. 1995. Behavior of vertical drain improved subsoil under embankment loading. Soils and Foundations, **35**(4): 49–61.

Chu, J., Yan, W., and Yang, H. 2000. Soil improvement by the vacuum preloading method for an oil storage station. Géotechnique, **50**(6): 625–632.

Cooper, M.R., and Rose, A.N. 1999. Stone column support for an embankment on deep alluvial soils. Proceedings of the Institution of Civil Engineers, Geotechnical Engineering, **137**(1): 15–25.

Gabr, M.A., and Szabo, D.J. 1997. Prefabricated vertical drains zone of influence under vacuum in clayey soil. *In* In Situ Remediation of the Geoenvironment: Proceedings of the Conference Held in Minneapolis, Minnesota, on 5–8 October 1997. *Edited by* J.C. Evans. American Society of Civil Engineers, Geotechnical Special Publication 71, pp. 449–460.

Hansbo, S. 1981. Consolidation of fine-grained soils by prefabricated drains and lime column installation. *In* Proceedings of 10th International Conference on Soil Mechanics and Foundation Engineering, Stockholm, 15–19 June 1981. A.A. Balkema, Rotterdam, The Netherlands. Vol. 3, pp. 677–682.

Hansbo, S. 1997. Aspects of vertical drain design: Darcian or non-Darcian flow. Géotechnique, **47**(5): 983–992.

Hird, C.C., Pyrah, I.C., and Russel, D. 1992. Finite element modeling of vertical drains beneath embankments on soft ground. Géotechnique, **42**(3): 499–511.

Holtz, R.D., Jamiolkowski, M.B., Lancellotta, R., and Pedroni, R. 1991. Prefabricated vertical drains: design and performance. CIRIA Report, Butterworth-Heinemann, London, UK. 131 pp.

Indraratna, B., and Redana, I.W. 1997. Plane strain modeling of smear effects associated with vertical drains. Journal of Geotechnical and Geoenvironmental Engineering, ASCE, **123**(5): 474–478.

Indraratna, B., and Redana, I.W. 2000. Numerical modeling of vertical drains with smear and well resistance installed in soft clay. Canadian Geotechnical Journal, **37**: 132–145.

Indraratna, B., Balasubramaniam, A.S., and Sivaneswaran, N. 1997. Analysis of settlement and lateral deformation of soft clay foundation beneath two full-scale embankments. International Journal for Numerical and Analytical Methods in Geomechanics, **21**: 599–618.

Indraratna, B., Redana, I.W., and Balasubramaniam, A.S. 1999. Settlement prediction of embankments stabilised with prefabricated vertical drains at Second Bangkok International Airport. *In* Geotechnical Engineering for Transportation Infrastructure: Theory and Practice, Planning and Design, Construction and Maintenance: Proceedings of the 12th European Conference on Soil Mechanics and Geotechnical Engineering, Amsterdam, The Netherlands, 7–10 June 1999. *Edited by* F.B.J. Barends, J. Lindenberg, H.J. Luger, L. de Quelerij, and A. Verruijt. A.A. Balkema, Rotterdam, The Netherlands. pp. 1–7.

Indraratna, B., Bamunawita, C., and Khabbaz, H. 2004. Numerical modeling of vacuum preloading and field applications. Canadian Geotechnical Journal, **41**: 1098–1110.

Mohamedelhassan, E., and Shang, J.Q. 2002. Vacuum and surcharge combined one-dimensional consolidation of clay soils. Canadian Geotechnical Journal, **39**: 1126–1138.

Nicholson, D.P., and Jardine, R.J. 1982. Performance of vertical drains at Queenborough bypass. *In* Vertical drains. *Edited by* I.R. Wood. The Institution of Civil Engineers, London, UK. pp. 67–90.

Richart, F.E. 1957. A review of the theories for sand drains. Journal of the Soil Mechanics and Foundations Division, ASCE, **83**(3): 1–38.

Shang, J.Q., Tang, M., and Miao, Z. 1998. Vacuum preloading consolidation of reclaimed land: a case study. Canadian Geotechnical Journal, **35**: 740–749.

Tang, M., and Shang, J.Q. 2000. Vacuum preloading consolidation of Yaoqiang Airport runway. Géotechnique, **50**(6): 613–623.

List of symbols

a width of the prefabricated vertical drain (m)
A cross-sectional area corresponding to flow (m^2)
b thickness of the prefabricated vertical drain (m)
b_s half-width of the smear zone
b_w half-width of the drain wall (m)
B half-width of the plane strain unit cell (m)
c_h coefficient of consolidation for horizontal drainage, $c_h = k_h/\gamma_w m_v$ (m^2/s)
d drain spacing (m)
d_e diameter of influence zone (m)
d_s smear diameter
d_w equivalent drain diameter
k permeability coefficient of soil (m/s)
k_h horizontal permeability coefficient in undisturbed zone (m/s)
k_s horizontal permeability coefficient in smear zone (m/s)
k_1 ratio between vacuum pressure at the bottom and top of the vertical drain
l length of drain (m)
m_v coefficient of volume compressibility for one-dimensional compression (m^2/kN)
n ratio r_e/r_w in axisymmetric condition or B/b_w in plane strain condition
p_0 applied vacuum pressure at the top of the drain (kN/m^2)
q_w well discharge capacity (m^3/s)
Q flow in unit cell (m^3)
Q_r flow in the r direction
Q_z flow in the z direction
r distance from centre of the drain in axisymmetric unit cell (m)
r_e radius of influence zone (m)
r_s radius of smear zone
r_w radius of drain well (m)
s ratio r_s/r_w in axisymmetric condition or B/b_s in plane strain condition
S settlement (m)
S_{novac} final settlement due to surcharge preloading only (m)
S_{vac} settlement due to surcharge with vacuum preloading (m)
t time (s, days)
T_h dimensionless time factor for horizontal drainage ($T_{h,ax} = c_h t/d_e^2$ or $T_{h,ps} = c_h t/4B^2$)
u excess pore-water pressure (kN/m^2)
u_s excess pore pressure in the smear zone
$\bar{u}$ average excess pore-water pressure for the unit cell (kN/m^2)
$\bar{u}_\infty$ average applied vacuum pressure for the unit cell (kN/m^2)
U_h average degree of consolidation
V volume of soil mass (m^3)
VPR vacuum pressure ratio (= p_0/σ_1)
x distance from centre of the drain in plane strain unit cell (m)
z depth (m)
α geometric parameter representing the influence zone
β geometric parameter representing the smear effect
θ geometric parameter representing the well resistance
ε vertical strain
γ_w unit weight of water (kN/m^3)
μ_{ax} group of parameters representing the geometry of the vertical drain system including well resistance and smear effect in the axisymmetric condition
μ_{ps} group of parameters representing the geometry of the vertical drain system including well resistance and smear effect in the plane strain condition
ν Poisson's ratio in terms of effective stress
σ_1 initial overburden pressure due to preloading (kN/m^2)
σ' effective stress (kN/m^2)

Subscripts

ax axisymmetric condition
ps plane strain condition
s smear zone

Appendix A. Complete details of analytical formulation of vacuum preloading for the plane strain condition

The horizontal flow rate in the unit cell can be expressed by Darcy's law as

$$[\text{A1}] \quad \frac{\partial Q}{\partial t} = \frac{k}{\gamma_w}\frac{\partial u}{\partial x}\,\mathrm{d}z$$

where A is the cross-sectional area of the flow at distance x which is equal to dz (the thickness of the unit cell for plane strain conditions is unity).

The rate of changing volume of soil mass is

$$[\text{A2}] \quad \frac{\partial V}{\partial t} = \frac{\partial \varepsilon}{\partial t}(B-x)\,\mathrm{d}z$$

The radial flow rate in the unit cell is equal to the rate of volume change of the soil mass in the vertical direction, and therefore

$$[\text{A3}] \quad \frac{k_{\text{h,ps}}}{\gamma_w}\frac{\partial u}{\partial x}\,\mathrm{d}z = \frac{\partial \varepsilon}{\partial t}(B-x)\,\mathrm{d}z$$

Rearranging eq. [A3], the excess pore pressure gradient outside the smear zone can be given by

$$[\text{A4}] \quad \frac{\partial u}{\partial x} = \frac{\gamma_w}{k_{\text{h,ps}}}\frac{\partial \varepsilon}{\partial t}(B-x) \qquad \text{for } b_s \le x \le B$$

The corresponding pore pressure gradient in the smear zone is derived as

$$[\text{A5}] \quad \frac{\partial u_s}{\partial x} = \frac{\gamma_w}{k_{\text{s,ps}}}\frac{\partial \varepsilon}{\partial t}(B-x) \qquad \text{for } b_w \le x \le b_s$$

Considering the horizontal cross-sectional slice of thickness dz (Fig. 2c), the change of flow in the z direction of the drain from the entrance to the exit of the slice dQ_z is expressed by

$$[\text{A6}] \quad \mathrm{d}Q_z = \frac{q_{\text{w,ps}}}{\gamma_w}\frac{\partial^2 u}{\partial z^2}\,\mathrm{d}z\,\mathrm{d}t \qquad \text{for } x \le b_w$$

The horizontal inflow to the drain from each slide dQ_x is given by

$$[\text{A7}] \quad \mathrm{d}Q_x = \frac{k_{\text{s,ps}}}{\gamma_w}\frac{\partial u}{\partial x}\,\mathrm{d}z\,\mathrm{d}t \qquad \text{for } x = b_w$$

If the water is assumed to be incompressible, the following equation should be satisfied:

$$[\text{A8}] \quad \mathrm{d}Q_z + 2\mathrm{d}Q_x = 0$$

At the drain boundary ($x = b_w$), the sudden drop in pore pressure does not take place, hence $u = u_s$. Substituting eqs. [A6] and [A7] in eq. [A8] and rearranging with the aforementioned boundary condition yields

$$[\text{A9}] \quad \left(\frac{q_{\text{w,ps}}}{2k_{\text{s,ps}}}\frac{\partial^2 u_s}{\partial z^2}\right)_{x=b_w} + \left(\frac{\partial u_s}{\partial x}\right)_{x=b_w} = 0$$

Integrating eq. [A9] in the z direction and subject to the boundary conditions (i) at $z = 0$, $u_s = -p_{0,\text{pl}}$ (applied vacuum pressure) and (ii) at $z = l$, $\partial u_s/\partial z = p_{0,\text{pl}}(1-k_1)/l$, the excess pore pressure at $x = b_w$, after substituting eq. [A5] into eq. [A9], can be determined by

$$[\text{A10}] \quad (u_s)_{x=b_w} = -p_{0,\text{ax}}\left[1-(1-k_1)\frac{z}{l}\right] + \frac{2(B-b_w)\gamma_w}{q_{\text{w,ps}}}\frac{\partial \varepsilon}{\partial t}\left(lz - \frac{z^2}{2}\right)$$

Integrating eqs. [A4] and [A5] in the x direction with the boundary conditions given in eq. [A10] and by assuming $u_s = u$ at the interface $x = b_s$ (see Fig. 2c), u and u_s can be expressed by

$$[\text{A11}] \quad u_s = \frac{\gamma_w}{2k_{\text{s,ps}}}\frac{\partial \varepsilon}{\partial t}\left[x(2B-x) + \frac{2(B-b_w)k_{\text{s,ps}}}{q_{\text{w,ps}}}(2lz - z^2) - b_w(2B-b_w)\right] - p_{0,\text{ps}}\left[1-(1-k_1)\frac{z}{l}\right] \qquad \text{for } b_w \le x \le b_s$$

$$[\text{A12}] \quad u = \frac{\gamma_w}{2}\frac{\partial \varepsilon}{\partial t}\frac{1}{k_{\text{h,ps}}}\left[x(2B-x) + \frac{2(B-b_w)}{q_{\text{w,ps}}} \times k_{\text{h,ps}}(2lz - z^2) - b_s(2B-b_s) - b_s(2B-b_s) + \frac{k_{\text{h,ps}}}{k_{\text{s,ps}}} \times (b_s - b_w)(2B - b_s - b_w)\right] - p_{0,ps}\left[1-(1-k_1)\frac{z}{l}\right] \qquad \text{for } b_s \le x \le B$$

The mean excess pore pressure ($\bar{u}$) is determined from

$$[\text{A13}] \quad \bar{u}(B-b_w)l = \int_0^l\int_{b_w}^{b_s} u_s\,\mathrm{d}x\,\mathrm{d}z + \int_0^l\int_{b_s}^{B} u\,\mathrm{d}x\,\mathrm{d}z$$

After substituting eqs. [A11] and [A12] into eq. [A13] and integrating eq. [A13], the average excess pore pressure is given by

$$[\text{A14}] \quad \bar{u} = \frac{B^2\gamma_w}{2k_{\text{h,ps}}}\frac{\partial \varepsilon}{\partial t}\mu_{\text{ps}} - p_{0,\text{ps}}\left[\frac{(1+k_1)}{2}\right]$$

where

$$\mu_{\text{ps}} = \left[\alpha + \frac{k_{\text{h,ps}}}{k_{\text{s,ps}}}(\beta) + \theta\right]$$

$$\alpha = \frac{2}{3}\frac{(n-s)^3}{n^2(n-1)}$$

$$\beta = \frac{2(s-1)}{n^2(n-1)}\left[n(n-s-1) + \frac{1}{3}(s^2+s+1)\right]$$

and

$$\theta = \frac{4k_{\text{h,ps}}}{3Bq_{\text{w,ps}}}\left(1-\frac{1}{n}\right)l^2$$

Combining eq. [A14] with the well-known compressibility relationship $\partial\varepsilon/\partial t = -m_v\,\partial\bar{u}/\partial t$ gives

$$[A15]\quad \bar{u} = -\frac{\gamma_w}{2k_{h,ps}} m_v \frac{\partial \bar{u}}{\partial t} B^2 \mu_{ps} - p_{0,ps}\left[\frac{(1+k_1)}{2}\right]$$

Rearranging eq. [A15] and then integrating by applying the boundary condition $\bar{u} = \sigma_1$ at $t = 0$ gives

$$[A16]\quad \frac{\bar{u}}{\sigma_1} = \left[1 + p_{0,ps}\frac{(1+k_1)}{2\sigma_1}\right]\exp\left(\frac{-8T_{h,ps}}{\mu_{ps}}\right) - p_{0,ps}\frac{(1+k_1)}{2\sigma_1}$$